Journal Name

ARTICLE

Dinuclear Rhenium pyridazine complexes containing bridging chalcogenide anions: synthesis, characterization and computational study

Received 00th January 20xx,
Accepted 00th January 20xx

DOI: 10.1039/x0xx00000x

www.rsc.org/

Lorenzo Veronese,[a,b] Elsa Quartapelle Procopio,[a] Daniela Maggioni,[a,c] Pierluigi Mercandelli,[*,a,c] Monica Panigati[*,a,b,c]

The synthesis of a series of neutral dinuclear rhenium complexes of general formula $[Re_2(\mu\text{-}ER)_2(CO)_6(\mu\text{-}pydz)]$ (pydz = pyridazine; E = S, Se or Te; R = methyl or phenyl; the TeMe is not included) has been carried out via new, either one-pot or two-step, procedures. The one-pot synthesis consists in the oxidative addition of RE-ER across the Re-Re bond of $[Re_2(CO)_{10}]$, in the presence of 1 equivalent of pyridazine, and affords the corresponding dinuclear complexes in high yields (ca. 85%). Furthermore, a general two-step procedure has been carried out, which involves the synthesis of heterocubane-like $[Re_4(\mu_3\text{-}ER)_4(CO)_{12}]$ molecules and their reaction with pyridazine, quantitatively affording the corresponding dinuclear species through a symmetric *[2+2]* fragmentation pathway. The molecular structure of the complexes has been elucidated by single crystal XRD analysis, and TD-DFT calculations have predicted the existence of conformers differing in the orientation of the chalcogen substituents with respect to the pyridazine ligand. The relative stabilities and the activation barriers for the interconversion have been calculated, observing a regular trend that has been rationalized in dependence on the hybridization of the chalcogen atom. Variable temperature NMR studies experimentally confirmed the theoretical prediction, showing, in solution, two conformers with different relative amounts and different interconversion rates between them, in dependence on the chalcogen nature. From the electrochemical point of view the S, Se and Te complexes display a bi-electronic reversible oxidation peak, differently from the two mono-electronic irreversible oxidation peaks previously observed for the O derivatives. Moreover, a progressive narrowing of the HOMO-LUMO gap going from O to Te, arising from the increase of the HOMO level, has been observed. This is in line with the decreasing electron-withdrawing strength of the chalcogenide bridging ligand, so that the energy gap for the telluride derivative is 1.64 eV, the smallest value in the whole family of the di-rhenium pyridazine complexes. The spectroscopic HOMO-LUMO gap parallels this trend, with a significant red-shift of the metal-to-ligand charge transfer absorption, making the telluride complex highly promising as photosensitizer in the field of solar energy conversion. In agreement with the narrow HOMO-LUMO gap, no photoluminescence has been observed upon optical excitation.

Introduction

The conversion from solar to electrical energy or the storage of solar energy into chemical bonds are very attractive strategies to produce and store carbon-free energy. From the molecular point of view, the key active component is the photocatalyst (for fuel production) or the photosensitizer (for the light conversion into current), which has to be a multi-functional system, able to perform in series several distinct acts.[1]
A general requirement for the molecules employed in these devices is the absorption in the visible region. This is the case of several metal complexes, used as photosensitizers in solar cells, characterized by intense absorption bands having metal-to-ligand charge transfer (MLCT) character.[2] These excited states, which rapidly decay into excited states having triplet manifold, usually survive enough to allow the charge transfer to suitable substrates, avoiding the charge recombination to the ground state.[3]

Recently we have reported some dinuclear rhenium complexes as sensitizers for Dye Sensitized Solar Cells (DSSCs), having general formula $[Re_2(\mu\text{-}X)(\mu\text{-}Y)(CO)_6(\mu\text{-pydz-4-COOH})]$, (with X = halide or hydride and Y = halide or carboxylate, pydz = pyridazine). Light-to-current conversion was indeed observed, although with moderate efficiency.[4] These complexes show absorption maxima in the range 405-443 nm, arising from MLCT transitions, when absorbed on TiO_2 film. They belong to the family of dinuclear rhenium complexes that contain two "$Re(CO)_3$" units connected by a bridging

[a] Dipartimento di Chimica, Università degli Studi di Milano, Via Golgi, 19, 20133 Milano, Italy..
[b] Istituto per lo Studio delle Macromolecole, Consiglio Nazionale delle Ricerche (ISMAC-CNR), Via E. Bassini, 15, 20133 Milano, Italy.
[c] Consorzio Interuniversitario Nazionale per la Scienza e Tecnologia dei Materiali (INSTM), Via G. Giusti 9, 50121 Firenze, Italy.
Electronic Supplementary Information (ESI) available. See
DOI: 10.1039/x0xx00000x

pyridazine ligand and two anionic ancillary ligands, such as halides,[5] hydrides,[6] carboxylates,[4] alcohoxides or sulfides.[7] In these complexes the LUMO orbitals are localized on the diazine ligand, while the HOMO orbitals are mainly localized on the "Re(μ-X)(μ-Y)Re" core, so that it is possible to tune the energy-gap by modifying the nature of both the ancillary ligands and the diazine substituents.[8]

Computational studies at TD-DFT level and experimental data showed that complexes containing one hydrido and one carboxylato ancillary ligands, or two thiophenolate ligands display the narrowest HOMO-LUMO gap and thus the widest absorption in the visible region.[4,7]

These features prompted us to investigate the optical properties of complexes containing the other chalcogenide anions as ancillary ligands. In the literature only a few examples of chalcogen-bridged rhenium complexes are available to date. Hupp and co-workers reported the synthesis of the sulfide bridged dinuclear rhenium complex $[Re_2(\mu\text{-}SPh)_2(CO)_8]$ from $[Re(CO)_5(OTf)]$ and thiols.[9] In the same report they also mentioned the stepwise syntheses of selenium bridged rhenium dimers $[Re_2(\mu\text{-}SeR)_2(CO)_8]$ from $[Re(CO)_5(OTf)]$ and selenols. The dinuclear $[Re_2(\mu\text{-}SPh)_2(CO)_8]$ complex had been previously obtained by oxidative addition of diaryl disulfide to the Re-Re bond of $[Re_2(CO)_{10}]$ under photolytic (and in much lower yields under thermolytic) conditions.[10] A similar approach has been more recently used to prepare $[Re_2(\mu\text{-}EPh)_2(CO)_6(L)_2]$ complexes (L = pyridine ligand, E = S[11] or Se[12]), by one-pot reaction of $[Re_2(CO)_{10}]$ with diaryl disulfides or diselenides, in the presence of pyridyl ligands. With rigid bidentate bi-pyridine ligands, tetranuclear selenium bridged metallacyclophanes $[Re_2(\mu\text{-}SeR)_2(CO)_6]_2(\mu\text{-}L)_2$ were obtained.[13]

The above reported literature data have been exploited here to establish a simple and effective general route to $[Re_2(\mu\text{-}ER)_2(CO)_6(\mu\text{-pydz})]$ complexes (E = S, Se or Te; R = phenyl or methyl, see Chart 1; TeMe is not included), by oxidative addition of E_2R_2 dichalcogenides to $[Re_2(CO)_{10}]$, in the presence of pyridazine ligand. This route does not apply to the corresponding phenolato and methanolato derivatives, due to the instability of the diphenylperoxide under the reaction conditions, and the commercial unavailability of the dimethylperoxide. Therefore, these complexes have to be prepared by the already reported synthetic procedures.[7]

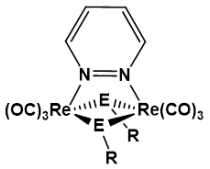

1a: E = O, R = Ph
1b: E = O, R = Me
2a: E = S, R = Ph
2b: E = S, R = Me
3a: E = Se, R = Ph
3b: E = Se, R = Me
4a: E = Te, R = Ph

Chart 1. A schematic view of the molecular structure of the investigated chalcogenide complexes.

In addition to the one-pot synthesis, a general two-step procedure has been also investigated. It involves as intermediate the chalcogen-bridged cubane-like $[Re_4(\mu_3\text{-}OH)_4(CO)_{12}]$ complexes, obtained by oxidative addition of E-E bonds on $[Re_2(CO)_{10}]$.[14]

All the complexes have been fully characterized from the theoretical and computational points of view. The spectroscopic properties of the complexes have been correlated to their molecular structure and, in particular, to the nature of the ancillary ligands, which can modulate the HOMO levels and the efficiency of light harvesting.

Results and discussion

Synthesis of the complexes

The previously reported[7] synthetic routes to $[Re_2(\mu\text{-}ER)_2(CO)_6(\mu\text{-pydz})]$ complexes (E = O or S; R = phenyl or methyl) were more complex than those used for the related dihalide $[Re_2(\mu\text{-}X)_2(CO)_6(\mu\text{-1,2-diazine})]$ complexes (X = Cl, Br or I),[5,8] because of the unavailability of the $[Re(CO)_5ER]$ precursors, analogous to the $[Re(CO)_5X]$ starting materials.

As already mentioned in the Introduction, we have therefore developed a general procedure for the synthesis of $[Re_2(\mu\text{-}ER)_2(CO)_6(\mu\text{-pydz})]$ complexes (E = S, Se or Te; R = phenyl or methyl), based on the self-assembly of five components, by the so called *orthogonal-bonding* approach, already employed for the synthesis of rhenium-based di- and tetra-nuclear derivatives.[11,12,15,16] The one-pot procedure involves the oxidative addition of the E_2R_2 ligand to $[Re_2(CO)_{10}]$, with substitution of one CO ligand for each metal centre, and further substitution of two axial CO groups, orthogonal to the first ones, by the bridging pyridazine ligand. The reaction occurs in toluene (or mesitylene for complexes **3** and **4**) solution at high temperature and affords the corresponding dinuclear complexes in high yields (ca. 85%, Scheme 1). The methyl-telluride derivative was not prepared, because the dimethylditelluride precursor is hardly commercially available, its preparation is not straightforward, and, above all, it was not strictly necessary to establish the correlations between the properties of the complexes and the nature of the chalcogen atom or of its substituents.

This approach cannot be used for the syntheses of the analogous derivatives containing halides as ancillary ligands, because in the reaction conditions the halogen molecules can react, in a parallel way, with the N-donor ligand. Actually, the oxidative addition of X_2 on $[Re_2(CO)_{10}]$ occurs in much milder conditions, affording $[Re(CO)_5X]$ (or $[Re_2(\mu\text{-}X)_2(CO)_8]$, depending on the reaction temperature), which can then react with the diazine, at high temperature, according to equation 1. This is the normal synthetic route to the dihalide complexes.[5]

$$2\ [Re(CO)_5X] + \text{diazine} \rightarrow [Re_2(\mu\text{-}X)_2(CO)_6(\mu\text{-diazine})] + 4\ CO \quad (X = \text{halide}) \quad (1)$$

In addition, we have investigated the possibility to extend to these chalcogenide derivatives the already established method for the synthesis of $[Re_2(\mu\text{-}OH)_2(CO)_6(\mu\text{-pydz})]$ (Scheme 2),[7] which involves the heterocubane-like $[Re_4(\mu_3\text{-}OH)_4(CO)_{12}]$ intermediate (equation 2).

$$[Re_4(\mu_3\text{-}OH)_4(CO)_{12}] + 2\ \text{pydz} \rightarrow 2\ [Re_2(\mu\text{-}OH)_2(CO)_6(\mu\text{-pydz})] \quad (2)$$

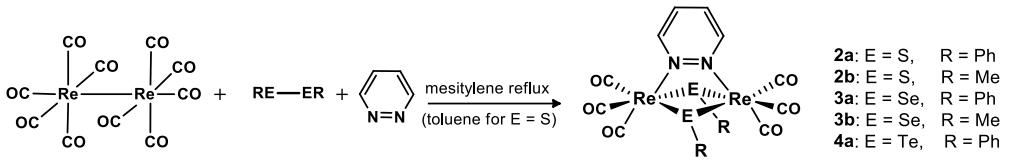

Scheme 1. The one-pot synthetic pathway for the complexes described.

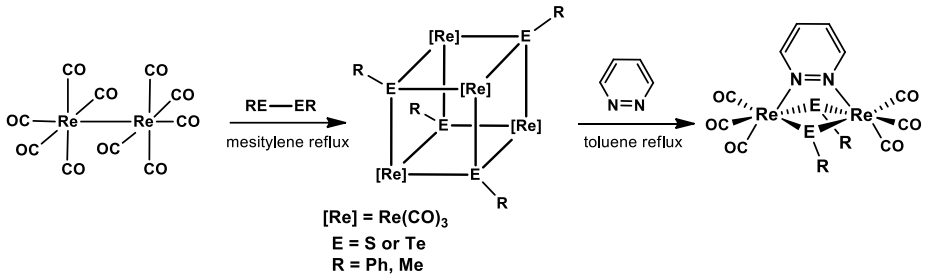

Scheme 2. The two-step synthetic procedure for the $[Re_2(\mu\text{-}ER)_2(CO)_6(\mu\text{-pydz})]$ complexes (E = S, Te, **2a** and **4a** respectively) *via* heterocubane structures.

Reaction 2 bears some resemblance with the previously reported fragmentation of the unsaturated tetranuclear cluster $[Re_4(\mu_3\text{-}H)_4(CO)_{12}]$ in the presence of 2 equivalents of pydz[6] that affords the $[Re_2(\mu\text{-}H)_2(CO)_6(\mu\text{-pydz})]$ complex, together with several other products. For the tetra-hydroxo derivative, on the contrary, only the *[2+2]* fragmentation pathway had been observed, quantitatively affording $[Re_2(\mu\text{-}OH)_2(CO)_6(\mu\text{-pydz})]$.[7] The applicability of the method has been investigated here for the SPh, SMe and TePh derivatives. The synthesis of $[Re_4(\mu_3\text{-}SPh)_4(CO)_{12}]$ had already been reported,[14] by oxidative addition of Ph_2S_2 to $[Re_2(CO)_{10}]$ in mesitylene solution. The same method has been used here to prepare the methyl sulfide and the phenyl telluride derivatives $[Re_4(\mu_3\text{-}SMe)_4(CO)_{12}]$ and $[Re_4(\mu_3\text{-}TePh)_4(CO)_{12}]$, respectively.

Differently from what observed for the sulfide derivatives,[14] in the case of telluride the reaction did not require the catalytic amount of dimethylformamide to promote the removal of carbonyl groups. However, in both cases the reaction yields are somewhat low (about 32%). The subsequent reaction of the cubane complexes with 2 equivalents of pyridazine in refluxing toluene quantitatively afforded complexes **2a**, **2b** and **4a** (Scheme 2). The nature of the new complexes was unambiguously established by a combination of spectroscopic and single-crystal X-ray characterization.

All the complexes display, in the ν(CO) region of the IR spectra, the typical four bands pattern of this class of compounds (see Table 1).[8] The position of these bands is affected by the d_π electron density on the metal centre, as a result of the π-back donation. Accordingly, the ν(CO) stretching modes of all the methyl derivatives are shifted to lower wavenumbers with respect to those observed for the analogous phenyl derivatives, in agreement with the stronger donating power of the corresponding anions. For the phenyl derivatives, the position of the highest-frequency A_1 mode shifts on varying the ancillary ligands, in the order 2036 (O-Ph) > 2035 (S-Ph) > 2032 (Se-Ph) > 2027 (Te-Ph) cm^{-1}. This trend is in agreement with the Re atoms becoming progressively more electron rich as the electronegativity of the E atoms decreases and with the partial delocalization of the t_{2g} orbitals over the phenyl moieties. The same trend is not observed for the analogous methyl derivatives due to the lack of such delocalization.

Solid state structures

The crystal structures of the μ-benzeneselenolato and μ-benzenetellurolato derivatives (**3a** and **4a**, respectively) have been determined. Figure 1 shows frontal and lateral views of the two new complexes **3a** and **4a**, along with the structures of the previously reported μ-phenolato and μ-benzenethiolato derivatives **1a** and **2a** for comparison.

Table 1. IR carbonyl stretching bands (in CH_2Cl_2, 298 K) of the investigated complexes.

Complex	IR ν (CO) [cm^{-1}]
1a (OPh)	2036 (m) 2021 (s) 1927 (s) 1903 (s)
2a (SPh)	2035 (m) 2018 (s) 1936 (s) 1911 (s)
3a (SePh)	2032 (m) 2016 (s) 1938 (s) 1910 (s)
4a (TePh)	2027 (m) 2011 (s) 1933 (s) 1912 (s)
1b (OMe)	2027 (m) 2010 (s) 1915 (s) 1892 (s)
2b (SMe)	2029 (m) 2011 (s) 1928 (s) 1914 (s)
3b (SeMe)	2027 (m) 2009 (s) 1930 (s) 1902 (s)

In the dinuclear species **3a** and **4a** each rhenium atom attains a distorted octahedral coordination and bears three terminal carbonyl ligands in a facial arrangement, one of the nitrogen atoms of the bridging pyridazine ligand, and the selenium (or tellurium) atoms of the two bridging benzeneselenolato (or benzenetellurolato) ligands. The two derivatives possess an idealized C_2 symmetry (not crystallographically imposed) unlike the μ-benzenethiolato

derivative **2a**, which is asymmetrical,[7] due to the different conformation adopted by the bridging groups (see Figure 1).

In spite of the decreasing Re–E–Re bond angle in the series **1a**–**4a** (103.8, 91.0, 88.2, and 84.0°, respectively), the Re–Re distance shows a constant elongation (3.35, 3.57, 3.66, and 3.73 Å, in the same order) as a consequence of the larger covalent radius of the bridging chalcogen atom. Indeed, the Re–E bond distance constantly increases along the series **1a**–**4a** (2.13, 2.50, 2.63, and 2.79 Å, respectively).[17]

The structural data gave important hint on the hybridization of the chalcogen atoms. In the case of μ-phenolato derivative **1a** the oxygen atoms show an almost exact trigonal planar coordination geometry (sum of the bond angles: 358.8°), suggesting the presence of an sp^2 hybridization for the oxygen atoms and a partial double-bond character for the Re–O bonds. At variance with this, the heaviest congeners clearly show a trigonal pyramidal coordination geometry. The sum of the bond angles around the chalcogen atom decreases along the series **2a**–**4a** (314.6, 305.6, and 296.0°, respectively), in agreement with the increasing p character of the hybridization of the bridging atom. As already observed for the thio-derivative **2a**, the pyramidal coordination of the chalcogen allows the phenyl substituents to lie outside the plane defined by the Re–(μ-E)–Re atoms, leading to the possible existence of geometric isomers in which the phenyl groups are directed either towards or away from the μ-pyridazine ligand (see Figure 1). In the symmetrical conformation adopted in the solid state by the selenium and tellurium derivatives **3a** and **4a** the phenyl substituents are both directed towards the pyridazine ligand (see the lateral views in Figure 1). However, the presence in solution of other isomers and the existence of dynamic processes responsible for their interconversion can be foreseen (see the Dynamic NMR characterization section).

Computational study

The family of chalcogenide-containing rhenium complexes was studied by means of density functional and time-dependent density functional (TD-DFT) computations.[18] Both the phenyl and the methyl substituted derivatives (**1a**–**4a** and **1b**–**4b**) were taken into account; however, the complete series of complexes has been prepared only for the species containing the EPh bridging ligands.

In the μ-phenolato and μ-methoxo complexes (**1a** and **1b**) the sp^2 hybridization of the bridging oxygen atoms constraints the molecule to assume a single conformation, showing the highest possible symmetry for these species (C_{2v}). In the heaviest congeners, however, the pyramidal geometry of the bridging chalcogen atoms allows the presence of more than one conformer, differing in the position of the two phenyl or methyl substituents with respect to the pyridazine ligand. For all the compounds, the more stable isomer is the one in which both the substituents are directed towards the pyridazine ligand (up,up conformer in Figure 2), while a less symmetric isomer, in which the two substituents are directed in opposite directions, lies higher in energy (up,down conformer).

A third isomer, with both the substituents directed away from the pyridazine ligand (down,down conformer), shows a significantly higher relative energy (see Table 2) and its actual presence can be ruled out.[19] The optimized structures of the (up,up) and (up,down) isomers of the μ-benzenethiolato complex **2a** are depicted in Figure 2, along with the transition structure for their interconversion. Relative stabilities and energy barriers for all the species are reported in Table 2.

The relative energy of both the (up,down) and (down,down) conformers with respect to the more stable (up,up) conformer increases on descending the group. This trend is particularly evident for the bulkier phenyl-substituted compounds, in which steric effects play a major role. On the contrary, energy barriers are higher for the methyl-substituted compounds, since in the μ-EPh complexes the transition structure is effectively stabilized by the conjugation between the phenyl ring and the sp^2-hybridized chalcogen atom (see the conformation assumed by the phenyl group in Figure 2, lower line).

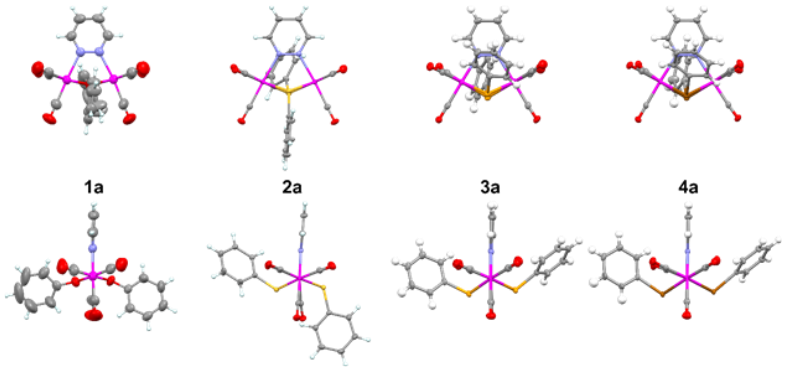

Figure 1. Crystal structures of $[Re_2(\mu\text{-EPh})_2(CO)_6(\mu\text{-pydz})]$ complexes **1a**–**4a** (E = O, S, Se, or Te): frontal and lateral views (upper line and lower line). Displacement ellipsoids are drawn at the 50% probability level. Color code: C, grey; H, white; N, blue; O, red; Re, magenta; S, yellow; Se, orange; and Te, brown. Data for complexes **1a** and **2a** are taken from ref. 7.

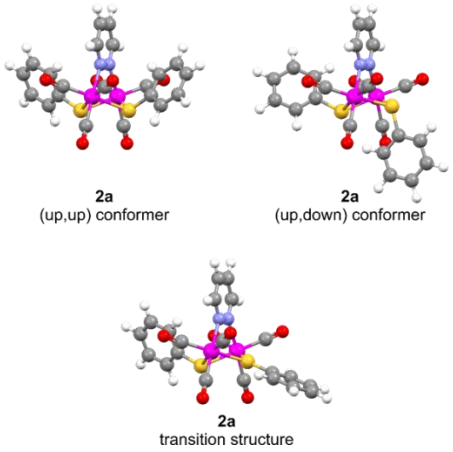

Figure 2. Molecular geometry of the (up,up), top left, and (up,down), top right, conformers for the complex $[Re_2(\mu\text{-SPh})_2(CO)_6(\mu\text{-pydz})]$ **2a**. The transition structure for their interconversion is depicted in the lower line.

Relative stabilities and energy barriers are further discussed in the Dynamic processes in solution section.

As previously found for analogous $[Re_2(\mu\text{-X})_2(CO)_6(\mu\text{-pydz})]$ complexes,[5,7] in these chalcogenide derivatives, LUMO and LUMO+1 are the two lowest-lying π* orbitals of the coordinated pyridazine. The following four MO (from LUMO+2 to LUMO+5) are the ''e_g'' set of the two Re atoms, showing, in addition, a large C≡O π* character.

For species **1b**–**4b** the six HOMOs are the ''t_{2g}'' set of the two Re atoms in a pseudo-octahedral environment. In particular, the three highest lying orbitals show a strong Re–(μ-E) π* character, in close analogy with the halogenated derivatives previously described. For species **1a**–**4a** ten HOMOs have to be taken into account, since the energy of the "t_{2g}" orbitals of the Re atoms are similar to those of the four highest lying π orbitals of the two phenyl groups of the μ-EPh bridging ligands. In addition, a partial mixing of these two types of MO is observed and some of the "t_{2g}" orbitals are partially delocalized over the phenyl moieties. Molecular orbital energies are listed in Table S1 in Supporting Information and partial orbital diagrams are depicted in Figure 3. Views of the most relevant molecular orbitals for complex **2b** are reported in Figure S1.

The absorption spectrum of all the complexes down to 230–250 nm was simulated by computing the lowest 40 singlet excitation energies, both *in vacuo* and in presence of dichloromethane. Selected transitions are reported in Table S2 and depicted in the diagrams of Figure 3. Results will be discussed in the Photophysical characterization section.

Table 2. Relative stability (ΔE)[a] for the different conformers of the complexes $[Re_2(\mu\text{-ER})_2(CO)_6(\mu\text{-pydz})]$ (E = S, Se or Te; R = Ph or Me) **2a**–**4a** and **2b**–**4b**, and energy barriers ($E^{\ddagger}$) for the interconversion between the (up,up) and the (up,down) conformers.

Complex	$\Delta E_{(up,down)}$ [kJ mol^{-1}]	$E^{\ddagger}$ [kJ mol^{-1}]	$\Delta E_{(down,down)}$ [kJ mol^{-1}]
2a (SPh)	1.5	37.7	15.6
3a (SePh)	5.9	63.8	25.0
4a (TePh)	8.0	87.9	30.0
2b (SMe)	2.5	52.0	15.0
3b (SeMe)	3.8	75.3	22.1
4b (TeMe)	3.9	93.0	22.4

Dynamic processes in solution by ^{1}H NMR

The variable temperature ^{1}H NMR spectra of the three phenyl derivatives **2a**, **3a** and **4a** are substantially different from each other. The same is observed for the two methyl derivatives **2b** and **3b**.

Phenyl derivatives. The spectrum of the telluride derivative **4a**, at all the investigated temperatures, clearly shows, in the aromatic region, two sets of sharp signals, with integrated intensity ratio 1 : 0.14 (see the traces in Figure 4). The two sets of signals can be attributed to the (up,up) and (up,down) conformers discussed in the Computational section.[20,21] In particular, the set of signals with the higher integrated intensities (in the order of increasing fields: H_{ortho} (pydz), H_{meta} (pydz), H_{para} (Ph), H_{ortho} (Ph), H_{meta} (Ph), relative ratio 1:1:1:2:2)

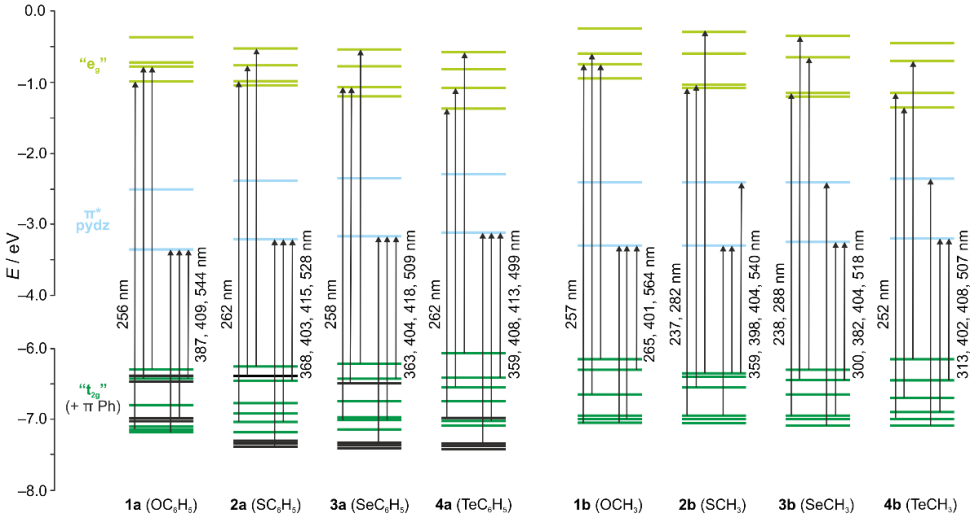

Figure 3. Partial molecular orbital diagram for the complexes $[Re_2(\mu\text{-ER})_2(CO)_6(\mu\text{-pydz})]$ (E = O, S, Se, or Te; R = Ph or Me) **1a**–**4a** and **1b**–**4b**. Orbitals are colored according to their main component: rhenium "t_{2g}" orbitals (dark green), pyridazine π* orbitals (light blue), rhenium "e_g" orbitals (light green), and phenyl π orbitals (black, in complexes **1a**–**4a**). Arrows correspond to electronic transitions involved in the absorption spectra (computed TD-DFT wavelength are given). In particular, for each species, values on the left and on the right refer to the d–d and the MLCT absorption, respectively (gas phase values).

is consistent with a C_2 symmetry isomer, in which free rotation around the Te-C_{hypso} bonds equalizes the *ortho* and *meta* positions within each phenyl ring.

A 2D ^{1}H NOESY experiment at 243 K (Figure 4) showed, for the major isomer (88%), the development of a n.O.e. cross peak between the signal of the *ortho* protons of the pyridazine ring and the signal of the *ortho* protons on the aryl rings, confirming unambiguously the attribution of this set of signals to the (up,up) isomer, with dynamic C_{2v} symmetry.

The set of signals with lower integrated intensities is compatible with the minor (up,down) isomer (estimated as the 12% of the total amount of the two isomers, on the base of the integrated intensity ratio 1 : 0.14). Also this conformer shows two pydz signals only (marked with an asterisk in Figure 4), because of the apparent C_s symmetry created by the free rotation around the Te-C_{hypso} bonds.

The invariance of the isomers ratio observed at different temperatures is attributable to kinetic factors, the interconversion rate being too slow to allow the fast attainment of the equilibrium during the variable temperature experiment (sharp multiplets are observed for both isomers even at 300 K).

Unlike what observed for **4a**, the spectra of **3a** and **2a** were significantly temperature-dependent (see Figures 5 and 6, respectively), suggesting the occurrence of dynamic processes interconverting different conformers. However, a different trend was observed for the two compounds.

In the case of the diselenide derivative **3a** (Figure 5), a limit spectrum, showing sharp multiplets for each isomer, could be observed only at temperatures below 233 K. The amount of the minor isomer was ca. 24% (from the 1 : 0.32 integration ratio at 233 K). At higher temperatures (273 K) the pyridazine resonances of the two isomers broadened and coalesced, affording two sharp averaged signals at room temperature. In the same temperature range the phenyl signals broadened and coalesced in one averaged signal, which remained very broad even at 300 K, in line with the larger chemical shift differences between the three couples of phenyl signals, requiring higher exchange rate for their averaging.

For the phenyl-sulfide complex **2a** (see Figure S2), the presence of two interconverting conformers was not clearly detectable. Evidence of the presence of a minor conformer was obtained only at very low temperatures (see the inset above the trace at 168 K of the stacked plot in Figure S2, which enhances 10× the intensity of spectrum in the range 6.6-8.5 ppm). Indeed at 168 K a slight broadening of the two pydz signals and especially the separation of the phenyl resonances were observed. This suggests that, even at such low temperature, the interconversion of the conformers of **2a** did not reach the slow exchange regime yet. For this reason the estimated amount of the minor isomer (ca. 40% at 168K) should be considered highly uncertain. From the above data, a progressive increase in the amount of the (up,down) conformer on passing from Te (12%) to Se (24%) to S (40%) can be argued in agreement with the computed energy differences between the (up,up) and (up,down) isomers, which increase on descending the group (1.5, 5.9 and 8.0 kJ mol^{-1}, for S, Se and Te, respectively, Table 2). However, the values of the isomer ratios have been estimated at different temperatures and, most of all, it is not granted (for kinetic reasons) that for all the temperatures they do correspond to true thermodynamic equilibrium ratios (see the above considerations about the Te derivative). Therefore, it cannot be stated with certainty that the experimental data provide firm support to the theoretical thermodynamic computations.

On the contrary, for the kinetic aspects of isomer interconversion, the experimental data give a well-grounded support to the DFT computations, since it is evidenced the increase of the activation barrier on going down the group (see the values of $E^{\ddagger}$ in Table 2). Indeed, from the above described spectra it is clear that the interconversion process becomes easier passing from Te to Se and then to S.

The Te derivative is in slow exchange regime on the NMR time scale even at 300 K, whereas the S derivative does not attain this limit even at 168 K. The Se compound displays an intermediate behaviour, showing averaged resonances at 300 K that separate in two distinct sets of signals at 233 K. This trend is attributable to the increasing sp^3 character of the orbital hybridization of the chalcogenide atoms on going from S to Se to Te, which implies a decrease of the Re-E-Ph angles along the series, and a concomitant raising of the steric crowding with the CO ligands. In all cases, the phenyl rings freely rotate around the S-C_{ipso} bond at any temperature, including the lowest ones.

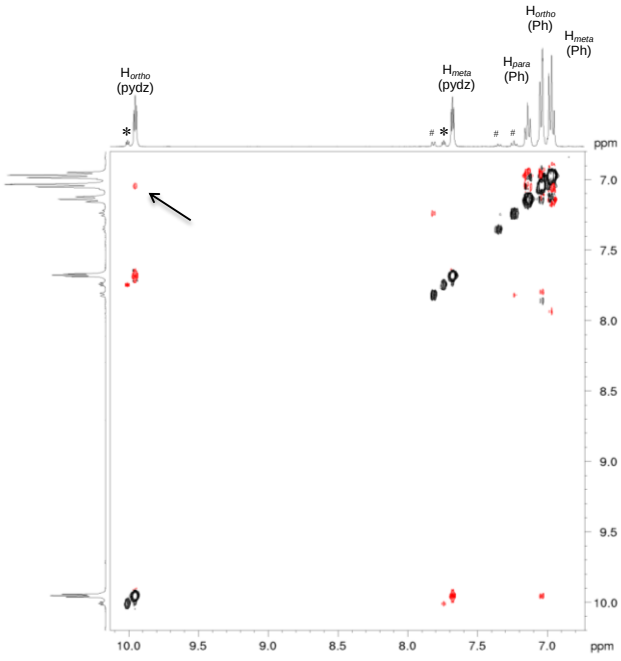

Figure 4. ^{1}H NOESY (243 K, CD_2Cl_2, 9.4 T) for ditelluride complex **4a**. The asterisk and the hash symbols mark the signals of pydz and of the downward phenyl ring, respectively, for the minor (up,down) isomer. The signals of the upward phenyl ring of the minor isomer are overlapped with the corresponding signals of the major (up,up) conformer. The arrow indicates the cross peak discussed in the text.

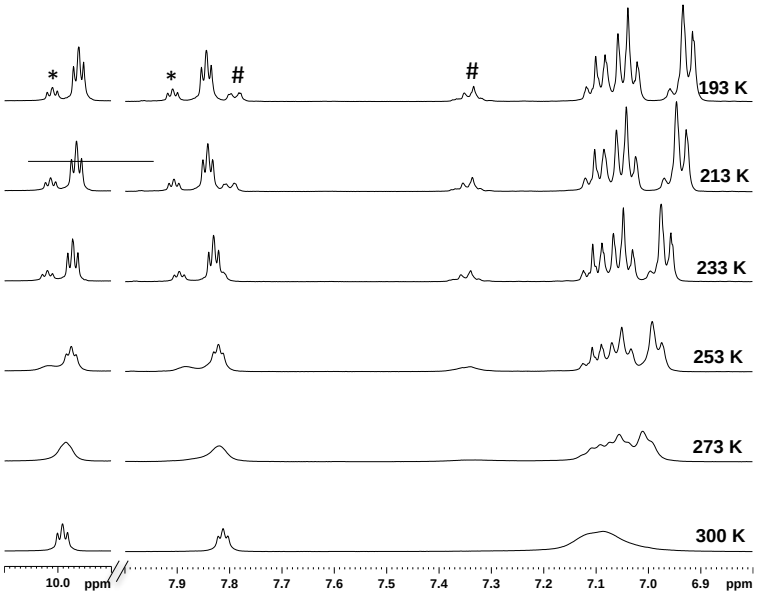

Figure 5. ^{1}H NMR at variable temperature for the SePh derivative **3a**. The peaks of pyridazine (*) and the downward phenyl ring (#, accidental overlap of *para* and *meta*) of the minor isomer are marked (CD_2Cl_2, 9.4 T).

Methyl derivatives. The presence in solution of the (up,up) and (up,down) conformers was observed for the two methyl derivatives **2b** and **3b** too. Also in this case, the isomer interconversion was faster for the S derivative with respect to the Se one, in agreement with the computed interconversion barriers ($E^{\ddagger}$ 52.0 vs 75.3 kJ mol^{-1} for **2b** and **3b**, respectively, Table 2). Actually, for **3b** separate (although broad) pyridazine and methyl signals of each conformer were observed already at room temperature (Figure S3), whereas for **2b** the signals of each conformer appeared well separated only at temperatures lower than 233 K (Figure 6). In both cases the minor isomers show two methyl resonances, that can be identified as the (up,down) species. For these conformers, the more shielded resonance lies very close to the unique signal of the major (up,up) species and can be therefore assigned to the up methyl group.

The comparison with the variable-temperature behaviour of the corresponding phenyl derivatives **2a** and **3a** confirms the higher rigidity of the methyl derivatives, discussed in the previous Computational section. Indeed, cooling to 253 K was necessary to detect the resonances of the minor isomer of the SePh derivative **3a**, as above described (see Figure 5), while for the SPh species **2a** the limiting spectrum was not attained even at 168 K (Figure S2).

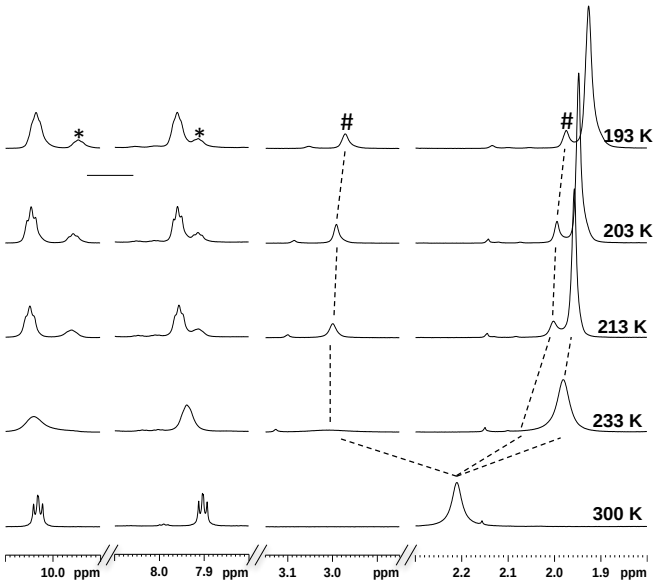

Figure 6. Selected aromatic and aliphatic regions of ^{1}H NMR variable temperature spectra of a solution of the SMe derivative **2b** (CD_2Cl_2, 9.4 T). The peaks of pyridazine (*) and the methyl moieties (#) of the minor isomer are marked.

Unlike the phenyl derivatives, for **2b** and **3b** the measured ratio between the (up,up) and (up,down) conformers was not significantly different, the minor isomer being ca. 25% for **2b** and 23% for **3b**, at 233 K (although for the latter the exchange kinetics is very likely too slow to ensure the attainment of equilibrium). This agrees with the small energy difference between the conformers computed for the methyl derivatives (2.5 and 3.8 kJ mol^{-1}, for **2b** and **3b** respectively, Table 2).

Electrochemical characterization

Figure 7 shows the results of cyclic voltammetry (CV) analyses of the complexes in acetonitrile (ACN) solution, while the most significant CV features are reported in Table 3. The first reduction peaks are localized, for all complexes, on the pyridazine ligand, as already observed for related complexes,[5a,7,8] and therefore occur at quite similar potential values. The reduction is monoelectronic and reversible, both from the chemical point of view (symmetrical return peaks, stable products) and from the electrochemical one (easy transfer of a single electron, which is taken into account by the ~57 mV half-peak widths together with the almost-zero E_p vs log v slopes), thus indicating very fast formation of a stable radical anion.

In the previous studies on similar complexes,[5a,8] the first oxidation site was found to be localized on the metal core, and therefore it was strongly affected by the nature of the ancillary ligands, as confirmed also by the DFT computations. In particular, a very different behaviour in the oxidation process was observed between the complexes containing OR$^-$ or SR$^-$ anions.[7] The complex with the SPh ligands (**2a**) showed one bielectronic oxidation, chemically and electrochemically reversible, as observed in the halide derivatives. On the contrary, in the OPh and OMe derivatives (**1a** and **1b**) a close sequence of two monoelectronic peaks was observed (as reported in Figure 7). In the case of the OMe derivative **1b**, the first oxidation peak tends to be chemically irreversible, at low scan rates, while the phenolato complex **1a** shows a combination of an irreversible first peak followed by a reversible second peak, in the whole scan rate range explored.[7]

The behaviour of the new chalcogenide derivatives here reported is completely similar to that of **2a**. One oxidation peak is observed, with neat ~30 mV width. This indicates that it corresponds to a bielectronic oxidation, in which a simultaneous two-electron transfer occurs, rather than two monoelectronic processes, as in the OR derivatives.[5a,8]

The values of the oxidation potentials strongly decrease in the O, S, Se, Te series (see Table 3), in agreement with the decreasing electronegativity on going down the group 16. The oxidation potential of the methyl derivatives **1b**-**3b** are lower than those of the corresponding phenyl complexes **1a**-**3a**, as expected for the stronger donating power of the EMe anions compared to the EPh ones.

An interesting correlation is observed plotting the peak potential values vs the wavenumbers of the ν(CO) stretching modes at the highest frequency, which are reliable indicators of the electron density on the metal atoms (see Figure 8).

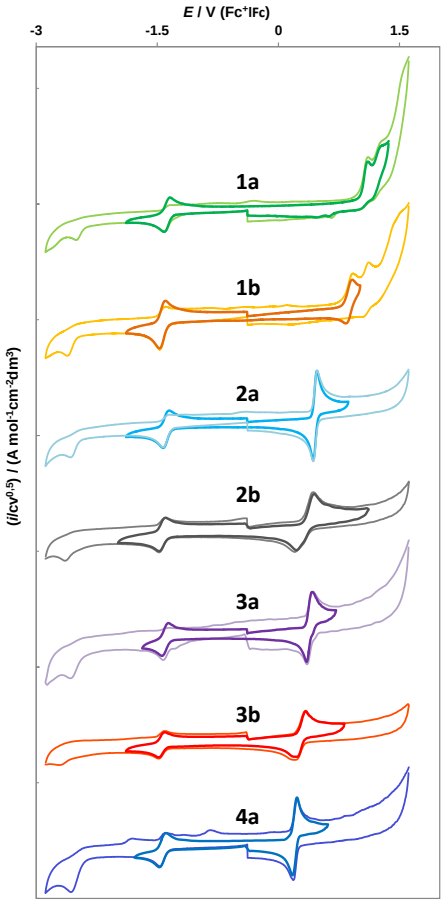

Figure 7. Full scan (thin line) and HOMO-LUMO (bold line) CV curves for the complexes here described (in the conditions of Table 3).

Table 3. First reduction and oxidation peak potentials ($E_{p,c}$ and $E_{p,a}$) and electrochemical (ΔE_e) and spectroscopic (ΔE_s)[a] energy gaps of the complexes **1**-**4**. Potentials are referred to the Fc$^+$|Fc couple[b] in the operating medium (ACN, 0.1 M $TBAPF_6$, TBA = tetrabutylammonium). Scan rate 0.2 V s^{-1}.

Complex	ER	E_{pc} [V]	E_{pa} [V]	E_{LUMO} [eV]	E_{HOMO} [eV]	ΔE_e [eV]	ΔE_s [eV]
1a	OPh	–1.416	1.100	–3.38	–5.90	2.52	3.38
2a	SPh	–1.431	0.473	–3.37	–5.27	1.90	3.07
3a	SePh	–1.403	0.385	–3.40	–5.18	1.78	2.95
4a	TePh	–1.429	0.212	–3.37	–5.01	1.64	2.82
1b	OMe	–1.475	0.911	–3.33	–5.71	2.39	3.36
2b	SMe	–1.440	0.332	–3.36	–5.13	1.77	3.12
3b	SeMe	–1.446	0.250	–3.35	–5.05	1.70	3.05

[a] The spectroscopic (ΔE_s) energy gaps is the energy associated to the electronic transition determined from the maximum of the MLCT absorption band. [b] Fc$^+$|Fc potential is 0.385 V vs SCE in acetonitrile solution.

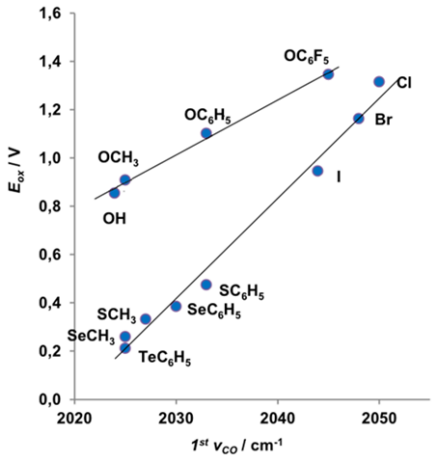

Figure 8. Plot of the first oxidation peak (in ACN) versus the wavenumbers of the highest energy ν(CO) band (in ACN).

The chalcogenide derivatives roughly follow the same trend of the halide ones, whereas the OR derivatives lie on a totally different line. This behaviour could be related to the hard-soft nature of the bridging ancillary ligands. Indeed, the softer SR^-, SeR^- and TeR^- anions can better stabilize the cationic products, favouring the simultaneous loss of two electrons instead of two mono-electronic oxidations, as observed in the case of the harder OR^- anions.

The last columns of Table 3 report the electrochemical and the spectroscopic HOMO–LUMO gaps. Both the trends parallel the trend of the first oxidation potential, and decreases from **1** to **4**, so that the energy gap for the TePh derivative **4a** is the smallest in the series.

Photophysical characterization.

The UV-Vis absorption spectra of all the complexes in diluted dichloromethane solution are shown in Figure 9, while the absorption peaks at the longest wavelengths are reported in Table 4, which also includes the data in acetonitrile solution.

At room temperature all the complexes exhibit an intense absorption band at high energy (about 270 nm) whose position is independent on the polarity of the solvent. In addition, a broad and featureless absorption band, with lower intensity, is observed for all the complexes. It covers a large part of the visible spectrum, between 350 nm and 550-600 nm, and its maximum shows a bathochromic shift on descending the group (which qualitatively parallels the shift to lower energy of the electrochemical HOMO-LUMO gap in the same series, see the previous paragraph). This band can be attributed to MLCT transitions, or, better, to metal-ligand-to-ligand charge transfer (MLLCT) transitions, due to the significant contribution of the ancillary ligands to the metal-centered HOMO set, shown by the above discussed DFT computations.[7] This broad band arises from the convolution of multiple transitions, as indicated by the TD-DFT computations (see Figure 3 and Table S2) and as experimentally testified by the more or less pronounced shoulders observed at longer wavelengths.

The charge transfer character of the low energy band is also supported by the observed solvatochromic behaviour. Indeed, a significant blue-shift of the absorption maximum has been observed in a more polar solvent, such as acetonitrile (see Table 4).

It is interesting to note that the absorption maxima of the methyl derivatives **2b** and **3b** are blue-shifted with respect to the corresponding phenyl derivatives **2a** and **3a**, in contrast with the position of the HOMO levels measured from the electrochemical data. These data strongly underline that, as already observed for other complexes of this family,[8] the electronic transitions responsible for the charge-transfer absorption band are not strictly HOMO-LUMO, but rather involve as starting orbitals the metal-centered HOMO-*n* set and, as final orbitals, the two low-lying π* orbitals of the diazine, (LUMO and LUMO+1, in agreement with the TD-DFT computations, Figure 3). In this contest it is worth mentioning that the complex $[Re_2(\mu\text{-H})(\mu\text{-4-OOC-TPA})(CO)_6(\mu\text{-pydz-4-COOH})]$ (TPA = diphenylaminobenzoato) previously used in dye-sensitized solar cells owing to its small HOMO-LUMO gap,[4] shows an absorption maximum strongly red-shifted with respect to **4a** (more than 50 nm, i.e. 487 nm vs 433 nm), in spite of the close ΔE_e similarity (1.64 eV for **4a** and 1.63 eV for the hydrido-carboxylate derivative).

Upon optical excitation at 450 nm at room temperature in CH_2Cl_2 solution, only the complexes with OR ancillary ligands (**1a** and **1b**) showed a broad and featureless emission band in the range 608-708 nm.[7] The emission for the other complexes **2**-**4** was instead completely negligible.

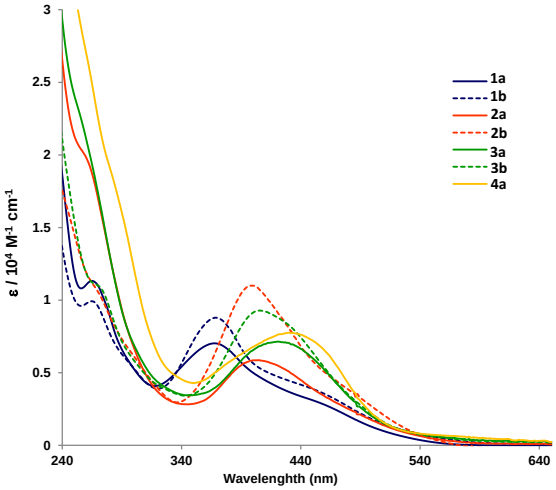

Figure 9. UV-Vis absorption spectra of the complexes here described, in CH_2Cl_2 solution.

Table 4. The lowest energy absorption band for complexes **1**-**4** in (a) CH_2Cl_2 solution and (b) ACN solution.

Complex	ER	$\lambda_{max}{}^a$ [nm]	ε^a [10^4 M^{-1} cm^{-1}]	$\lambda_{max}{}^b$ [nm]
1a	OPh	367	0.69	337
2a	SPh	403	0.57	382
3a	SePh	421	0.69	391
4a	TePh	433	0.71	396
1b	OMe	369	0.87	342
2b	SMe	397	1.10	375
3b	SeMe	406	0.85	382

Conclusions

A one-pot procedure has been developed, in which a Re(μ-ER)$_2$(μ-pyridazine-*k*^{2}*N,N'*)Re core, containing six new metal-ligand bonds, is formed in high yields, through a sequence that involves oxidative addition of R_2E_2 on [$Re_2(CO)_{10}$] and pyridazine coordination in bridging position. Two mutually orthogonal carbonyl ligands on each Re atom are eliminated during the reaction, as well as the direct Re-Re interaction.

In addition a synthetic procedure has been established in which the oxidative addition of R_2E_2 and the coordination of the diazine ligand occur in two separate steps. In the first one, heterocubane-like [$Re_4(\mu_3\text{-ER})_4(CO)_{12}$] complexes are formed and isolated, following a reaction path previously used for the preparation of sulfur-bridged derivatives.[14] The reaction is of interest by itself, because very few reports are available in the literature on the formation of this kind of tetrametallic cubanes, containing anions bridging on three metal centres. In the second step the $Re_4(\mu_3\text{-ER})_4$ core is cleaved by reaction with 1,2-diazines, to give the corresponding dinuclear complex, through a clean *[2+2]* fragmentation pathway. Therefore it has been further confirmed the hypothesis that the use of bidentate potentially bridging ligands might favor the symmetric *[2+2]* fragmentation, as already observed for the synthesis of the dihydroxo[7] and dihydrido[6] derivatives.

An interesting feature of these complexes is the possible existence of conformers differing in the orientation of the chalcogen substituents with respect to the pyridazine ligand. A combination of single crystal XRD analyses, DFT computation and NMR studies has been used to highlight this point. The presence in solution of interconverting conformers has been ascertained and the variable temperature NMR data have qualitatively validated the theoretical prediction. The factors responsible for the regular trends of the conformer ratio and of the interconversion rate have been rationalized on the grounds of the hybridization of the chalcogen atoms.

A complete electrochemical and photophysical investigation showed the progressive narrowing of the HOMO-LUMO gap going from O to Te, arising from an increase of the HOMO level. This is in line with the decrease of the electron-withdrawing strength of the chalcogenide bridging ligand, making the telluride complex **4a** highly promising as photosensitizer for solar cells. Actually, for **4a**, the HOMO level is more than 0.4 eV higher than that of the hydrido-carboxylato complex [Re_2(μ-H)(μ-4-OOC-TPA)$(CO)_6$(μ-pydz-4-COOH)], already used as dye sensitizer in operating DSSCs.[4]

Moreover, the possibility to tune the energy-gap for these species also by modifying the substituents on the diazine will allow to further stabilize the LUMO level by using diazine ligands containing electron-withdrawing substituents. In this way the energy gap could be further reduced, thus improving the light harvesting ability. Finally, it must be taken into account the ease of preparation, which constitutes a not negligible aspect of the complexes here described with respect to the previously employed hydrido-carboxylato derivatives. We therefore expect that the products here described (and in particular the telluride derivative) may find applications in the field of solar energy conversion.

Experimental Section

General methods

All the reagents were purchased from Aldrich and used as received. All the reactions were performed under inert N_2 atmosphere. All the solvents were deoxygenated and dried by standard methods before use; toluene and mesitylene were distilled on $Na_{(s)}$, while CH_2Cl_2 on P_2O_5. Commercial deuterated solvents and ACN were used as received. Column chromatography was performed using Alfa Aesar silica gel 60 (0.032–0.063 mm). ^{1}H NMR spectra were recorded on a Bruker DRX-400 MHz instrument, equipped with a Bruker 5 mm BBI Z-gradient probe head with a maxima gradient strength of 53.5 G/cm. IR spectra in solution were acquired on a Bruker Vector 22 FT spectrophotometer. Electronic absorption spectra were recorded on an Agilent Model 8543 spectrophotometer at room temperature, and using quartz cells with 1.0 cm path length. The syntheses of the complexes **1a** and **1b** and of the cubane [$Re_4(\mu_3\text{-SPh})_4(CO)_{12}$] have been already reported in references 7 and 14 respectively.

Syntheses of the complexes

One-pot synthesis of [Re_2(μ-SPh)$_2(CO)_6$(μ-pydz)] (2a). The precursor [$Re_2(CO)_{10}$] (130 mg, 0.2 mmol) and diphenyldisulfide (43.5 mg, 0.2 mmol) were dissolved in anhydrous toluene (8 mL). Then, pyridazine (15 μL, 0.2 mmol) was added and the mixture stirred under reflux for 10 days, slowly turning black. The solution was evaporated to dryness under vacuum, and the residue was dissolved in CH_2Cl_2 and precipitated with *n*-hexane obtaining an orange solid. The precipitate was then washed with *n*-hexane (3 × 5 mL), yielding 150 mg (0.18 mmol) of orange powder (yield 89%). IR (CH_2Cl_2) ν(CO): 2034 (m), 2018 (vs), 1937 (s), 1911 (s) cm^{-1}, ^{1}H NMR: (CD_2Cl_2, 300 K, 400 MHz) δ_H (ppm) 9.97 (m, 2H, H_{ortho} pydz), 7.91 (m, 2H, H_{meta} pydz), 7.20-7.15 (m, 10H, phenyl). Elemental anal. calcd for $C_{22}H_{20}N_2O_6Re_2S_2$: C 31.27, H 2.39, N 3.32. Found: C 31.54, H 2.46, N 3.30.

One-pot synthesis of [Re_2(μ-SMe)$_2(CO)_6$(μ-pydz)] (2b). The precursor [$Re_2(CO)_{10}$] (100 mg, 0.15 mmol) was dissolved in 8 mL of anhydrous toluene. Then, dimethyldisulfide (14 μL, 0.15 mmol) and pyridazine (11 μL, 0.15 mmol) were added to the reaction mixture, which was stirred under reflux for 10 days. The solution was evaporated to dryness under vacuum, and the residue re-dissolved in CH_2Cl_2 and precipitated with *n*-hexane, obtaining an orange solid. The precipitate was washed with *n*-hexane (3 × 5 mL) and then purified through column chromatography (toluene/AcOEt 9:1) yielding 57 mg (0.068 mmol) of product (yield 52%). IR (CH_2Cl_2) ν(CO): 2029 (m), 2011 (vs), 1928 (s), 1904 (s) cm^{-1}, ^{1}H NMR: (CD_2Cl_2, 300K, 400 MHz) δ_H (ppm) 10.03 (m, 2H, H_{ortho} pydz), 7.90 (m, 2H, H_{meta} pydz), 2.21 (s, 6H, CH_3). Elemental anal. calcd for

$C_{12}H_{16}N_2O_6Re_2S_2$: C 20.00, H 2.24, N 3.89. Found: C 20.45, H 2.28, N 3.86.

One-pot synthesis of [Re_2(μ-SePh)$_2$(CO)$_6$(μ-pydz)] (3a). The precursor [$Re_2(CO)_{10}$] (100 mg, 0.15 mmol) and diphenyldiselenide (48 mg, 0.15 mmol) was dissolved in 7 mL of anhydrous mesitylene. Then, pyridazine (11 μL, 0.15 mmol) was added to the reaction mixture, which was stirred under reflux for 2 days, slowly turning dark brown. The solution was evaporated to dryness under reduced pressure. The dark orange crude product was dissolved in CH_2Cl_2 and precipitated with *n*-hexane. The precipitate was then washed with *n*-hexane (3 × 5 mL), yielding 116 mg (0.125 mmol) of microcrystalline powder (yield 82%). IR (CH_2Cl_2) ν(CO): 2032 (m), 2016 (vs), 1938 (s), 1910 (s) cm^{-1}, ^1H NMR: (CD_2Cl_2, 300K, 400 MHz) δ_H (ppm) 9.99 (m, 2H, H_{ortho} pydz), 7.81 (m, 2H, H_{meta} pydz), 7.4-6.8 (br, m, 10H, phenyl). Elemental anal. calcd for $C_{22}H_{20}N_2O_6Re_2Se_2$: C 28.15, H 2.15, N 2.98. Found: C 28.55, H 2.25, N 2.96.

One-pot synthesis of [Re_2(μ-SeMe)$_2$(CO)$_6$(μ-pydz)] (3b). The precursor [$Re_2(CO)_{10}$] (100 mg, 0.15 mmol) was dissolved in anhydrous mesitylene (7 mL). Then, dimethyldiselenide (15 μL, 0.15 mmol) and pyridazine (11 μL, 0.15 mmol) were added, and the reaction mixture stirred under reflux for 2 days. The solution was evaporated to dryness under vacuum. The crude solid was dissolved in CH_2Cl_2 and precipitated with *n*-hexane. The precipitate was then washed with *n*-hexane (3 × 5 mL). The resulting powder was slowly recrystallized from CH_2Cl_2/*n*-hexane yielding 45 mg (0.055 mmol) of product (yield 36 %). IR (CH_2Cl_2) ν(CO): 2027 (m), 2009 (vs), 1930 (s), 1902 (s) cm^{-1}, ^1H NMR: (CD_2Cl_2, 300K, 400 MHz) major isomer δ_H (ppm) 10.09 (m, 2H, H_{ortho} pydz), 7.84 (m, 2H, H_{meta} pydz), 1.78 ppm (s, 6H, CH_3); minor isomer δ_H (ppm) 10.04 (m, 2H, H_{ortho} pydz), 7.83 (m, 2H, H_{meta} pydz), 2.73 ppm (s, 3H, $CH_{3\ down}$), 1.80 ppm (s, 3H, $CH_{3\ up}$);. Elemental anal. calcd for $C_{12}H_{16}N_2O_6Re_2Se_2$: C 17.69, H 1.98, N 3.44. Found: C 17.73, H 1.98, N 3.42.

One-pot synthesis of [Re_2(μ-TePh)$_2$(CO)$_6$(μ-pydz)] (4a). The precursor [$Re_2(CO)_{10}$] (100 mg, 0.15 mmol) and diphenylditelluride (63 mg, 0.15 mmol) were dissolved in anhydrous mesitylene (8 mL). Then, pyridazine (11 μL, 0.15 mmol) was added, and the reaction mixture was stirred under reflux for 1 day, slowly turning black. The solution was evaporated to dryness under reduced pressure. The dark red solid residue was dissolved in CH_2Cl_2 and precipitated with *n*-hexane. The crude product was then washed with *n*-hexane (3 × 5 mL) and then purified through column chromatography (CH_2Cl_2/*n*-hexane 8:2) yielding 113 mg (0.11 mmol) of microcrystalline powder (yield 72%). IR (CH_2Cl_2) ν(CO): 2027 (m), 2011 (vs), 1933 (s), 1912 (s) cm^{-1}, ^1H NMR: (CD_2Cl_2, 300K, 400 MHz) major isomer δH (ppm) 9.96 (m, 2H, H_{ortho} pydz), 7.65 (m, 2H, H_{meta} pydz), 7.15 ppm (m, 2H, CH_{para} phenyls), 7.10 ppm (m, 4H, CH_{ortho} phenyls), 6.98 ppm (m, 4H, CH_{meta} phenyls); minor isomer δH (ppm) 10.01 (m, 2H, H_{ortho} pydz), 7.85 (m, 2H, CH_{ortho} phenyl down), 7.71 (m, 2H, H_{meta} pydz), 7.35 (m, 1H, CH_{para} phenyl down), 7.24 (m, 2H, CH_{meta} phenyl down) 7.15 (m, 1H, CH_{para} phenyl up), 7.10 ppm (m, 2H, CH_{ortho} phenyl up), 6.98 ppm (m, 2H, CH_{meta} phenyl up). Elemental anal. calcd for $C_{22}H_{20}N_2O_6Re_2Te_2$: C 25.50, H 1.95, N 2.70. Found: C 25.48 H 1.96, N 2.68.

Synthesis of [Re_4(μ$_3$-SMe)$_4$(CO)$_{12}$]. The precursor [$Re_2(CO)_{10}$] (75 mg, 0.115 mmol) and dimethyldisulfide (10.2 μL, 0.115 mmol) were dissolved in anhydrous toluene (6 mL). Then, 50 μL of dimethylformamide were added to the reaction mixture that was stirred under reflux overnight. The solution was evaporated to dryness under vacuum. The dark brown crude product was purified through column chromatography (CH_2Cl_2/*n*-hexane 8:2) yielding 17 mg (0.014 mmol) of product (yield 23%). IR (CH_2Cl_2) ν(CO): 2029 (s), 1942 (s) cm^{-1}, ^1H NMR: (CD_2Cl_2, 300K, 400 MHz) δ_H (ppm) 2.08 (m, 12H, CH_3). Elemental anal. calcd for $C_{16}H_{12}O_{12}Re_4S_4$: C 15.14, H 0.95. Found: C 15.60, H 1.05.

Synthesis of [Re_4(μ$_3$-TePh)$_4$(CO)$_{12}$]. The precursor [$Re_2(CO)_{10}$] (125 mg, 0.19 mmol) and diphenylditelluride (78 mg, 0.19 mmol) were dissolved in anhydrous mesitylene (8 mL). The reaction mixture was stirred under reflux for 6 days. The solution was evaporated to dryness under vacuum. Then, the dark brown solid residue was dissolved in CH_2Cl_2 and precipitated with *n*-hexane. The precipitate was washed with *n*-hexane (3 × 5 mL), yielding 60 mg (0.032 mmol) of product (yield 32%). IR (CH_2Cl_2) ν(CO): 2025 (s), 1936 (m) cm^{-1}, ^1H NMR: (CD_2Cl_2, 300K, 400 MHz) δ_H (ppm) 7.50 (m, 24H). Elemental anal. calcd for $C_{36}H_{20}O_{12}Re_4Te_4$: C 22.76, H 1.06. Found: C 23.03, H 1.13.

Synthesis of 2a, 2b and 4a from the corresponding cubane complexes. For the synthesis of **2a**, the cubane cluster [Re_4(μ$_3$-SPh)$_4$(CO)$_{12}$] (30.3 mg, 0.020 mmol) was dissolved in anhydrous toluene (10 mL), and added with 2.9 μL of pyridazine (0.039 mmol). The mixture was stirred under reflux overnight turning red. The solution was evaporated to dryness under vacuum. The dark orange solid product was purified through column chromatography (CH_2Cl_2/*n*-hexane 8:2) yielding 20.3 mg (0.024 mmol) of microcrystalline powder of **2a** (yield 60%). The same procedure was followed for the preparation of **2b** and **4a**, with isolated yields of 66% and 77%, respectively (in the latter case chromatographic purification was not performed.

Electrochemical measurements

The cyclovoltammetric study of the complexes was performed at scan rates typically ranging from 0.02 to 10 Vs^{-1} in HPLC-grade acetonitrile (ACN) solutions at 2.5×10^{-4} M concentration in each substrate, deaerated by N_2 bubbling, with 0.1 M $TBAPF_6$ (Aldrich, TBA = NBu_4) as the supporting electrolyte, at 298 K. The ohmic drop was compensated by the positive feedback technique. The experiments were carried out using an AUTOLAB PGSTAT potentiostat (EcoChemie, The Netherlands) run by a PC with GPES software. The working electrode was a glassy carbon one (AMEL, diameter 1.5 mm) cleaned by diamond powder (Aldrich, diameter 1 mm) on a wet cloth (STRUERS DP-NAP); the counter electrode was a platinum wire; the reference electrode was an aqueous saturated calomel electrode, having in our working medium a

difference of +0.385 V vs. the $Fc^+|Fc$ couple (the intersolvent redox potential reference currently recommended by IUPAC).

Single-crystal X-ray diffraction analysis

Crystal data for ***3a***·*x*CH_2Cl_2. $C_{22+x}H_{14+2x}Cl_{2x}N_2O_6Re_2Se_2$, x = 0.036(2), M_r = 935.77, monoclinic, space group $P2_1/n$ (No. 14), a = 11.6624(8), b = 18.0556(13), c = 11.5828(8) Å, β = 94.0070(10)°, V = 2433.0(3) Å^3, Z = 4, d_{calc} = 2.555 g cm^{-3}, T = 150(2) K, crystal size = 0.105 × 0.055 × 0.045 mm^3, μ = 12.982, λ = 0.71073 Å. Refinement of 315 parameters on 6433 independent reflections out of 46670 measured reflections (R_{int} = 0.0313, $R_σ$ = 0.0212, $2θ_{max}$ = 59.2°) led to R_1 = 0.0205 (I > 2σ(I)), wR_2 = 0.0427 (all data), and S = 1.032, with the largest peak and hole of 2.547 and −1.453 e Å^{-3}. The disordered dichloromethane molecule was modeled isotropically employing a soft restraint on the C-Cl bond distances. Its occupation factor was refined to a value of 0.036(2). The cell chosen to describe **3a** is not in its standard form, in order to emphasize the isostructural relationship between **3a** and **4a**.

Crystal data for ***4a***·½CH_2Cl_2. $C_{22.5}H_{15}ClN_2O_6Re_2Te_2$, M_r = 1072.41, monoclinic, space group $P2_1/n$ (No. 14), a = 11.7418(5), b = 18.5045(8), c = 12.0354(5) Å, β = 93.4940(10)°, V = 2610.14(19) Å^3, Z = 4, d_{calc} = 2.729 g cm^{-3}, T = 150(2) K, crystal size = 0.16 × 0.11 × 0.10 mm^3, μ = 11.601, λ = 0.71073 Å. Refinement of 325 parameters on 6970 independent reflections out of 47577 measured reflections (R_{int} = 0.0318, $R_σ$ = 0.0180, $2θ_{max}$ = 59.1°) led to R_1 = 0.0162 (I > 2σ(I)), wR_2 = 0.0361 (all data), and S = 1.142, with the largest peak and hole of 1.576 and −1.914 e Å^{-3}. The disordered dichloromethane molecule was modeled anisotropically employing a soft restraint on the C-Cl bond distances.

CCDC-1534148 and 1534149 contains the crystallographic data for **3a** and **4a**. These data can be obtained free of charge from The Cambridge Crystallographic Data Centre.

Computational details

Ground state geometries were optimized by means of density functional calculations. The parameter-free hybrid functional PBE0[22] was employed along with the standard valence double-ζ polarized basis set 6-31G(d,p) for C, H, Cl, N, O, and S. For Re, Se, and Te the Stuttgart-Dresden effective core potentials were employed along with the corresponding valence triple-ζ basis set (SDD) and a set of polarization functions on Se and Te ($α_{d,Se}$ = 0.338, $α_{d,Te}$ = 0.237).[23]All the calculations were done assuming the symmetry described in the text, in particular the most stable conformer of **1a** and **1b**-**4b** possess C_{2v} symmetry while the most stable conformer of **2a**-**4a** possess C_2 symmetry. The nature of all the stationary points was checked by computing vibrational frequencies and all the species were found to be true minima (stable conformers) or first-order saddle points (transition states). In order to simulate the absorption electronic spectrum down to 230-250 nm the lowest 40 singlet excitation energies were computed by means of time-dependent density functional calculations. Calculations were done also in presence of solvent (dichloromethane, used in most of the photophysical characterizations) described by the polarizable continuum model (PCM) using the integral equation formalism variant.[24] All the calculations were done with Gaussian 09.[25]

Conflicts of interest

There are no conflicts of interest to declare.

Acknowledgements

M. P. and P. M. thank the Italian Ministero dell'Istruzione, Università e Ricerca, for financial support (PRIN-2012A4Z2RY). The use of instrumentation purchased through the Regione Lombardia – Fondazione Cariplo joint SmartMatLab Project (2013-1766) is gratefully acknowledged.

Notes and references

1 Y. Pellegrin and F. Odobel, *Coord. Chem. Rev*., 2011, **255**, 2578–2593.
2 (a) B. Bozic-Weber, E. C. Constable and C. E. Housecroft, *Coord. Chem. Rev.,* 2013, **257**, 3089–3106; (b) M. Nazeeruddin, A. Kay, I. Rodicio, R. Humphry-Baker, E. Müller, P. Liska, N. Vlachopoulos and M. M. Grätzel, *J. Am. Chem. Soc.*, 1993, **115**, 6382–6390; (c) K. Kalyanasundaram and M. M. Grätzel, *Coord. Chem. Rev.*, 1998, **177**, 347–414.
3 (a) L. M. Kiefer, J. T. King and K. J. Kubarych, *Acc. Chem. Res.* 2015, **48**, 1123−1130; (b) S. Campagna, F. Puntoriero, F. Nastasi, G. Bergamini and V. Balzani, *in Photochemistry and Photophysics of Coordination Compounds I,* V. Balzani and S. Campagna, Eds.; Springer: Berlin Heidelberg, *Top Curr. Chem.* 2007, **280**, 117−214.
4 L. Veronese, E. Quartapelle Procopio, F. De Rossi, T. M. Brown, P. Mercandelli, P. Mussini, G. D'Alfonso and M. Panigati, *New. J. Chem.*, 2016, **40**, 2910−2919.
5 (a) D. Donghi, G. D'Alfonso, M. Mauro, M. Panigati, P. Mercandelli, A. Sironi, P. Mussini and L. D'Alfonso, *Inorg. Chem.*, 2008, **47**, 4243−4255; (b) M. Mauro, E. Quartapelle Procopio, Y. Sun, C.-H. Chien, D. Donghi, M. Panigati, P. Mercandelli, P. Mussini, G. D'Alfonso and L. De Cola, *Adv. Funct. Mater.,* 2009, **19**, 2607−2614; (c) M. Mauro, C.-H. Yang, C.-Y. Shin, M. Panigati, C.-H. Chang, G. D'Alfonso and L. De Cola, *Adv. Mater*., 2012, **24**, 2054−2058.
6 M. Panigati, D. Donghi, G. D'Alfonso, P. Mercandelli, A. Sironi and L. D'Alfonso, *Inorg. Chem.*, 2006, **45**, 10909−10921.
7 A. Raimondi, M. Panigati, D. Maggioni, L. D'Alfonso, P. Mercandelli, P. Mussini and G. D'Alfonso, *Inorg. Chem.,* 2012, **51**, 2966–2975.
8 M. Panigati, M. Mauro, D. Donghi, P. Mercandelli, P. Mussini, L. De Cola and G. D'Alfonso, *Coord. Chem. Rev*., 2012, **256**, 1621–1643.
9 K. D. Benkstein, J. T. Hupp and C. L. Stern, *Inorg. Chem.,* 1998, **37**, 5404−5405.
10 F. Calderazzo, R. Poli and P. F. Zanazzi, *Inorg. Chem.,* 1991, **30**, 3942−3947.
11 A. Vanitha, P. Sathiya, S. Sangilipandi, S. M. Mobin and B. Manimaran, *J. Organomet. Chem.,* 2010, **695**, 1458−1463.
12 A. Vanitha, S. M. Mobin and B. Manimaran, *J. Organomet. Chem.*, 2011, **696**, 1609−1617.
13 B. Manimaran, A. Vanitha, M. Karthikeyan, B. Ramakrishna and S. M. Mobin, *Organometallics,* 2014, **33**, 465−472.

14 M. Karthikeyan and B. Manimaran, *J. Organomet. Chem.*, 2014, **769**, 130−135.
15 M. Sathiyendiran, R. T. Liao, P. Thanasekaran, T. T. Luo, N. S. Venkataramanan, G. H. Lee, S. M. Peng and K. L. Lu, *Inorg. Chem.,* 2006, **45**, 10052−10054.
16 R. T. Liao, W. C. Yang, P. Thanasekaran, C. C. Tsai, M. Sathiyendiran, Y. H. Liu, T. Rajendran, H. M. Lin, T. W. Tseng and K. L. Lu, *Chem. Commun.,* 2008, 3175−3177.
17 Geometric parameters found in **3a** and **4a** are unexceptional and similar to those reported for the few analogous species containing a Re-(μ-SeR)-Re or a Re-(μ-TeR)-Re fragment (Cambridge Structural Database 5.37). Bond distances and angles reported in the text are average values; the largest standard uncertainty on individual bond distances and angles are 0.005 Å and 0.4°, respectively.
18 Results on complexes **1a** and **1b** are taken from our previous work (ref. 7), apart from the simulation of the absorption electronic spectrum in presence of dichloromethane, due to the introduction of a new algorithm for PCM solvation in the release of the program employed in this work.
19 For the phenyl substituted derivatives **2a**-**4a** the (up,up), (up,down), and (down,down) conformers possess C_2, C_1 and C_s symmetry, respectively; while for the methyl substituted derivatives **2b**-**4b** the (up,up) and (up,down) conformers possess C_{2v} and C_s symmetry, respectively. The (down,down) conformers of **2b**, **3b**, and **4b** possess C_{2v}, C_2, and C_s symmetry, respectively.
20 The presence of isomers was previously recognized for the somewhat related derivatives $[Fe_2(\mu\text{-}SR)_2(CO)_6]$, but their interconversion was not investigated.[21]
21 E. Kostiner, M. L. N. Reddy, D. S. Urch and A. G. Massey, *J. Organomet. Chem.,* 1968, **15**, 383−395.
22 Called PBE1PBE in Gaussian. (a) C. Adamo and V. Barone, *J. Chem. Phys.,* 1999, **111**, 6158–6170; (b) J. P. Perdew, K. Burke and M. Ernzerhof, *Phys. Rev. Lett.,* 1996, **77**, 3865–3868; (c) J. P. Perdew, K. Burke and M. Ernzerhof, *Phys. Rev. Lett.,* 1997, **78**, 1396.
23 S. Huzinaga, J. Andzelm, M. Kłobukowski, E. Radzio-Andzelm, Y. Sakai and H. Tatewaki in Gaussian Basis Sets for Molecular Calculations; *Elsevier*: Amsterdam, 1984; p. 23.
24 J. Tomasi, B. Mennucci and R. Cammi, *Chem. Rev.,* 2005, **105**, 2999–3093.
25 Gaussian 09 (revision C.01), Gaussian Inc., Wallingford, CT, 2010.